Ultra-rapid metagenotyping of the human gut microbiome

Zhou Jason Shi[1,2], Boris Dimitrov[3], Chunyu Zhao[1], Stephen Nayfach[4,5,*] and Katherine S. Pollard[1,2,6,*]

[1]Chan Zuckerberg Biohub, Data Science, San Francisco, CA, [2]Gladstone Institutes, San Francisco, CA,
[3]Chan Zuckerberg Initiative, CA, [4]Department of Energy, Joint Genome Institute, Walnut Creek, CA,
[5]Lawrence Berkeley National Laboratory, Environmental Genomics and Systems Biology Division,
Berkeley, CA, [6]University of California San Francisco

*e-mail: snayfach@lbl.gov; katherine.pollard@gladstone.ucsf.edu

Abstract

Sequence variation is used to quantify population structure and identify genetic determinants of phenotypes that vary within species. In the human microbiome and other environments, single nucleotide polymorphisms (SNPs) are frequently detected by aligning metagenomic sequencing reads to catalogs of genes or genomes. But this requires high-performance computing and enough read coverage to distinguish SNPs from sequencing errors. We solved these problems by developing the GenoTyper for Prokaytotes (GT-Pro), a suite of novel methods to catalog SNPs from genomes and use exact k-mer matches to perform ultra-fast reference-based SNP calling from metagenomes. Compared to read alignment, GT-Pro is more accurate and two orders of magnitude faster. We discovered 104 million SNPs in 909 human gut species, characterized their global population structure, and tracked pathogenic strains. GT-Pro democratizes strain-level microbiome analysis by making it possible to genotype hundreds of metagenomes on a personal computer.

Software availability: GT-Pro is available at https://github.com/zjshi/gt-pro.

Introduction

Microbial species harbor extensive genetic variation, including single nucleotide polymorphisms (SNPs), structural variants (SVs), and mobile genetic elements. SNPs in particular are useful for population genetic analyses[1], such as tracking transmission of strains between environments or locations, reconstructing strain phylogenetic relationships, resolving mixtures of genotypes within a host, and depicting population diversity or structure along environmental gradients. Additionally, SNPs can result in changes in protein function. For example, a single SNP in the Dadh gene of the human commensal *Eggerthella lenta* can predict activity of levodopa, the primary medication used to treat Parkinson's disease[2]. Quantifying intra-species genomic variation in the human microbiome is a prerequisite to the potential application of microbiome genomics to precision medicine.

Several approaches exist for identifying SNPs in microbiomes. The gold standard[3] is to sequence individual isolate genomes and identify mismatches in whole-genome alignments. In contrast, metagenomes are a rich source of strain level diversity for uncultivated taxa. In a landmark study, Schloissnig et al[4]. discovered 10.3 million SNPs for 101 human gut species by aligning short reads from shotgun metagenomes to reference genomes. This approach is known as "metagenotyping" and has since been featured in several tools, including Constrains[5], MIDAS[6], metaSNV[7], DESMAN[8] and StrainPhlAn[9]. While algorithms for read alignment have improved, the approach is still computationally costly. Exact matching algorithms such as Kraken[10], CLARK[11] and bfMEM[12], have been developed as a more efficient solution to the read mapping problem, achieving speedups by orders of magnitude. However, these tools have thus far been used to quantify the abundance of microbiome taxa, rather than identify intra-species genetic variation. Genotyping by exact matches between reads and short sequences covering SNPs was implemented in the method LAVA[13] for human whole-genome sequencing data. Our goal was to extend this approach to metagenomes by addressing the challenges presented by complex mixtures of species and strains within microbiome samples, while also making software that could run on a personal computer.

Results

A novel framework for in silico *genotyping of microbiome species*

We introduce the GenoTyper for PROkaryotes (GT-Pro), which is a novel computational pipeline that utilizes an exact matching algorithm to perform ultra-rapid and accurate genotyping of known SNPs from metagenomes. Our proof-of-principle initial implementation of this approach focuses on the human gut microbiome. We created a reference database of 104 million common SNPs that we identified using 112,904 high-quality genomes from 909 human gut microbiome species. Then we used this catalog to perform reference-based SNP calling for 25,133 publicly available metagenomes, providing insight into strain variation across individuals and geographic regions. Our results demonstrate the feasibility of performing large-scale metagenotyping without need for high-performance computing.

To overcome the low throughput, sensitivity and species coverage of current alignment-based metagenotyping methods, we developed the GT-Pro framework (Fig. 1). Our key innovations are (i) capturing the majority of common variation found in microbiome genomes with a compact database of SNP covering k-mers (sck-mers), (ii) selecting highly species-specific sck-mers, overcoming high false positives associated with k-mer exact-matching methods, and (iii) developing and optimizing algorithms and data structures for exact matching of metagenomic sequencing reads to these sck-mers, enabling SNPs to be detected rapidly and accurately in microbiome samples. Building a version of GT-Pro for a given environment involves 1) discovering common SNPs in assembled genomes for each species, 2) optionally identifying linkage disequilibrium (LD) blocks and “tag” SNPs that capture most variation within each block, and 3) designing species-specific sck-mers. We focus on common SNPs) because this allows us to create a virtual genotyping “array” that is a data structure small enough to fit in computer memory while stll capturing the majority of prevalent genetic variation for each of many species.

A database of common SNPs for bacterial species in the gut microbiome

As a case study, we applied GT-Pro to the human gut microbiome due to the large number of microbial genomes from this environment and its important role in human health. To construct a SNP catalog, we used 112,904 high-quality genomes (>= 90% completeness and <= 5% contamination[14]) from 909 species (minimum = 10 genomes, median = 35 genomes) that we downloaded from the Unified Gastrointestinal Genomes (UHGG) resource[15] (Fig. S1, S2 and Table S1). These include both metagenome-assembled genomes[16–18] (i.e. MAGs, 94.1%) as well as cultivated isolates (5.9%) and were derived from geographically and phenotypically diverse human subjects. We performed whole-genome alignments for each species, revealing 104,171,172 common, core-genome SNPs (minor allele frequency >= 1%, site prevalence >= 90%), the vast majority of which (93.4%) were bi-allelic (Fig. 2a, S3a and S4). An extremely low fraction of SNPs (<0.2%) either disrupted a stop codon or introduced a premature one, which is one indicator of false positives (Fig. 2a). For context, this catalog is 10-fold larger than the one established by Schloissnig et al. and 1.22-fold larger than the catalogue of all human SNPs[19] (Fig. S1). Consistent with previous reports[4], SNP density, nucleotide diversity, and the rate of nonsynonymous versus synonymous mutations (pN/pS) varied across species and phyla (Fig. 2b and Fig. S5-8), which may reflect differences in selective pressures, population sizes, or transmission modes.

We hypothesized that the SNP database could be greatly compressed by clustering SNPs into linkage disequilibrium (LD) blocks that co-vary across reference genomes (Fig. S9) and selecting a single "tag"

SNP per LD block. A similar strategy is commonly used when designing genotyping arrays in human genetics. Using single-linkage clustering ($R^2 > 0.81$), the 104 million SNPs were clustered into 6.8 million LD blocks, representing a >15-fold reduction in database size and revealing a remarkable degree of local genomic structure. Our choice of R^2 is motivated by thresholds used for high confidence SNP imputation in other species and the fact that discovery of LD blocks stabilizes in this range for gut species (Fig. S10). On average LD blocks spanned ~4.3Kbp and ~23.5 SNPs, though the number and size of LD blocks varied considerably across bacterial species (Fig. 2c, S5c and S11a and b). As expected, linkage between SNPs decayed with increasing genomic distance (Fig. 2d-f), though decay rates differed substantially across species (Fig. 2d-e). Altogether, these differences in genetic diversity and structure across species likely reflect variation in recombination rates and/or the number and relatedness of sequenced genomes.

Species-specific kmers enable accurate and efficient identification of SNPs

Having constructed a large SNP catalog of the gut microbiome, we next used GT-Pro to identify k-mers that could unique identify each SNP from shotgun metagenomes. We empirically determined that length k=31 ensured high specificity while limiting compute and memory requirements. Of the ~13.3 billion candidate 31-mers that overlapped a SNP (124 per SNP), we identified 5.7 billion that were unique. These kmers overlapped 51% of the 104 million SNPs for 65% of LD blocks (mean 108 sck-mers per SNP, >1 sck-mer for 97% of species, Fig. S1 and S12). We refer to these as species-specific, SNP-covering kmers (sck-mers). Species with few or no SNPs that can be genotyped with this strategy include those with a very close relative and are most common within Actinobacteria (Fig. 2g and S3b). While only 50% of SNPs were tagged by a sck-mer, they capture 83% of the within species variation compared to whole-genome average nucleotide identity, and achieve a much higher level of resolution compared to individual taxonomic markers (Fig. S13). Due to the large scale of the database, GT-Pro uses a highly efficient data structure to store the sck-mers, requiring only 13 GB of RAM and permitting GT-Pro to run on most modern personal computers (Fig. S14 and S15). We also created a low memory version of the GT-Pro database (< 4 GB RAM) which just stores sck-mers for a single "tag" SNP per LD block (Methods) and still captures the majority of within species variation (Fig. S13).

Optimized k-mer exact matching accelerates metagenotyping 100-fold

To search for exact matches between billions of k-mers among metagenome reads and billions of sck-mers in the GT-Pro database, it is crucial to have a highly efficient search algorithm with low RAM and I/O requirements. To this end, we developed an exact match algorithm that leverages data structures optimized for this specific application (Fig. S16). Our approach is similar to a multi-index search with three main steps operating on bit encoded k-mers (2 bits per base) (Fig. S16a). After generating all k-mers in each metagenomic sequencing read, GT-Pro uses a l-bit Bloom filter on the first l<k bits of each k-mer to quickly rule out the vast majority of read k-mers that have no chance to match database sck-mers because they do not share an l-mer. For the k-mers that pass through the l-bit filter, the algorithm recruits an m-bit (last m bits of encoded k-mer) index to serve as secondary filter that locates a bucket of pre-sorted sck-mers in the database containing all possible exact matches to the full k-mer. Finally, the algorithm invokes a sequential search for exact matches between the full k-mer and these only the sck-mers in this bucket.

We next evaluated GT-Pro computational performance. First, we measured both speed and peak RAM use while tuning the values of l and m, two parameters derived from the l-bit and m-bit filter that are expected to have a large impact on performance due to their direct relationships with query speed and peak RAM use. In general, both performance metrics increase with higher values of l and m (Fig. 3a). Within the range of the tested parameters, we found best speed and peak RAM use with l = 30 and m = 35 in the laptop environment (26.5GB RAM) and the with l = 32 and m = 36 on a server (56.55 GB RAM). In a boundary case (l = 30 and m = 36) on the laptop where the peak RAM use hit the hardware limit, speed drops >87%. These results demonstrate that the values of l and m should be carefully chosen based on the hardware for optimal performance, which is handled automatically by GT-Pro.

We then compared the computational performance of GT-Pro to traditional read alignment method as baseline (Fig. 3b). We arbitrarily selected a total of 40 stool metagenomes from a Tanzanian cohort[20] (Table S7) for the evaluation. For alignment, SNPs were called mapping reads to database from GT-Pro and an independent one (metaSNV[7]). Although GT-pro had a larger peak RAM use than alignment method (<10GB), was 100x faster on a server and 10x faster on a laptop where peak RAM use was 26.5GB (Fig. 3b).

Accurate identification of SNPs from simulated metagenomes

We next evaluated the accuracy of SNP calling with GT-Pro compared to alignment using simulated metagenomes. Towards this goal, we generated Illumina sequencing reads *in silico* from 978 human gut isolates[21] and identified the ground truth set of SNPs based on whole-genome alignment. We first simulated reads from individual isolates with sequencing coverages ranging from 0.001x to 15x (Table S2). In this simplified scenario, genotyping errors can result from sequencing errors, insufficient coverage, or incorrect read or k-mer mapping. Across isolates and coverage levels, the false discovery rate (FDR) of genotypes was on average lower for GT-Pro (median= 0.7%, IQR=1.1%) compared to read alignment (median= 2.2%, IQR=4.7%) (Fig. 4a) while the median sensitivity of GT-Pro tended to be consistently higher (4.1-17.6%) at all coverages (Fig. 4b). While read alignment methods typically use a minimum coverage threshold to avoid false positives from sequencing error (e.g. >10x), that would have further decreased the sensitivity in this experiment.

Next, we simulated metagenomes containing pairs of conspecific isolates to evaluate performance on samples with strain mixtures, exploring a range of coverage ratios from 0.001x to 15x, where one strain is always at 15x coverage and the other varying (Table S3 and S4). In terms of detecting heterozygous sites (strains with different alleles), the false discovery rate (FDR) of GT-Pro (median= 0.9%, IQR=0.7%) was slightly higher compared to alignment (median= 0.3%, IQR=0.6%) (Fig. 4c), however, median sensitivity was higher (50.5-81.6%) for GT-Pro at all coverage ratios (Fig. 4d). A higher FDR for GT-Pro is likely caused by sequencing errors that match the alternative allele by chance, which also could cause a slightly lower sensitivity for GT-Pro at homozygous sites (Fig. S17).

To evaluate genotype calls imputed from tag SNPs, we found low FDR<5% comparing to true genotypes for the vast majority of isolates (>95%) (Fig. 4e). SNPs belonging to an LD block were 5 times more likely to be detected (non-zero read count) when their tag SNPs were also detected than when they were not (Fig. S18). To show that GT-Pro is highly quantitative, we compared average coverage at SNPs in the GT-Pro output to the known genome coverage using metagenomes we simulated from individual isolates and pairs of conspecific isolates. Even at low sequencing coverage (<1X), GT-Pro was able to accurately estimate the true coverage of each species (Fig. 4f) and the ratio between two strains (Fig. 4g). These results suggest that GT-Pro allele calls and counts could be used to impute genotypes and estimate relative abundances of species and strains accurately.

Accurate metagenotyping and gene imputation from gut metagenomes

To compare GT-Pro to existing approaches, we metagenotyped gut metagenomes[16,20,22,23] (Table S5-10) with alignment and compared the number of genotyped SNPs plus estimates of allele frequencies and genetic distances. We found that GT-Pro genotyped more species and SNPs per metagenome (Fig. S19a-c), despite being limited to species with ≥10 genomes. This is likely due to GT-Pro having better sensitivity for low coverage species and using a human gut focused database (comparing to metaSNV). For species genotyped by both methods, within-sample heterozygosity (Fig. S18) and across-sample allele presence and frequency (Fig. 5a-d) were highly correlated. For high coverage species, alignment method detected some SNPs absent from the GT-Pro database, whereas GT-Pro detected more sites as polymorphic in medium and low coverage species (Fig. 5a-d). Despite these differences in genotyped sites, GT-Pro and alignment produce highly similar estimates of pairwise genetic distances (Jaccard index) between samples, likely because rare variants missed by GT-Pro but with sufficient coverage to be genotyped with alignment-based methods represent a small fraction of overall genetic diversity. For comparison, we repeated this analysis using only SNPs in the 16S gene and observed much lower genetic differences between samples (Fig. S21), emphasizing that GT-Pro provides strain resolution close to that of alignment and greatly exceeding that of marker gene approaches. Altogether these results are consistent with our simulations and underscore the high sensitivity of GT-Pro.

Next, we sought to determine if GT-Pro SNPs could be used to infer the presence of nearby genes or operons, thereby serving as biomarkers for structural variants. As a case study, we used GT-Pro SNPs in flanking genes to predict presence/absence of toxicity controlling genes in *Clostridium difficile (C. difficile)*. We used the GT-Pro SNPs from two 5' (CD2601 and CD2602), one 3' (trpS) gene and intergenic region to train a Random Forest classifier to predict the presence of the genomic region (CdtLoc) of three toxin genes (CD196_cdtA, CD630_cdtAB and cdtR) in a set of *C. difficile* isolate genomes downloaded independently from NCBI (Fig. S22a and S23a). In another example, we demonstrated that SNPs (cdd2, cdu1, and intergenic) flanking a pathogenicity locus (PaLoc) region could predict its presence (Fig. S22b and S23b). Next we applied these models to GT-Pro metagenomes from 7,459 samples (Fig. 5e and f). Our predictions of CdtLoc and PaLoc region presence were highly correlated with estimated presence based on read alignment to the *C. difficile* genome, especially in metagenomes where this species was more abundant, and weaker predictions were made when not all of the genes in CdtLoc or PaLoc were present (Fig. S24a and b). These results show that GT-Pro can detect structural and strain variants when they are in high LD with flanking common SNPs.

Depicting novel and global intra-species genetic structure with GT-Pro

To evaluate the commonality of SNPs in GT-Pro database and how GT-Pro perform in metagenotying unknown metagenomes. We next used GT-Pro's common SNPs to perform dimension reduction on the genomes in the database as well as metagenomic samples from a North American IBD cohort[24] (n=220; Table S11) that did not contribute genomes to the GT-Pro database. Looking for evidence of subspecies genetic structure, we observed that for most species the metagenomes clustered with the genomes (Fig. 6a and b), suggesting that GT-Pro's database represents the common diversity across diverse metagenomes. For a few species, however, we observed clusters comprised only of metagenomes (Fig. 6c and d), demonstrating that novel subspecies genetic structure can be discovered using GT-Pro common SNPs.

Having shown GT-Pro is faster and at least as accurate as alignment-based methods for genotyping common SNPs from metagenomes, we leveraged GT-Pro metagenotypes to conduct the most geographically diverse intra-species genetic variation meta-analysis to date, encompassing 51.8 million SNPs for 881 species found in 7,459 gut samples from 31 locations across six continents (Table S13). Consistent with prior studies[4,6,9], we observed much less allele sharing between hosts (median=0.03, IQR=0.05) than within a host over time (median=0.38, IQR=0.4), and that intra-host allele sharing varies greatly between species and hosts (Fig. S25). Inter-host allele sharing differed across countries and continents (Fig. S26a and b), generally decreasing with geographic distance (Fig. S26a and b and S27a and b) and varying across species (Fig. S28). Our results also show clear associations with degree of industrialization as well as relatedness of hosts (e.g., hosts within villages in Fiji share more alleles than unrelated hosts in North American cities) (Fig. 6e). To identify gut species with high levels of inter-continental population differentiation, we calculated FST for 78 prevalent and well-detected (see methods) species and observed large differences in the degree of differentiation across species (Fig. 6f). Species with high FST show distinct clusters of hosts, some but not all of which correlate with geography (Fig 6g), consistent with lifestyle and environment playing a role in which strains colonize a host. In contrast, hosts do not cluster as clearly based on species relative abundance (Fig 6h), emphasizing that metagenotypes may reveal microbiome-host associations missed in abundance analyses.

Discussion

Here, we greatly extended the gut microbiome genomic variation landscape by identifying more than 100 million common core-genome SNPs from 909 bacterial species. As our solution to the bioinformatics challenge of metagenotyping, GT-Pro avoids computationally costly alignment and overcomes computing barriers. It performs strain-level analyses of microbiomes with improved accuracy, especially for low coverage species. Studies of microbiome genetic variation on a laptop or at the scale of human genome-wide association studies will be computationally feasible with GT-Pro.

It should be noted that our method comes with several limitations. First, the GT-Pro database does not capture all human gut microbial diversity. While we used 909 species, we could not use the majority of the UHGG species due to limited availability of high-quality genomes. Second, GT-Pro is analogous to a genotyping array and hence does not identify novel SNPs, which require other methods, such as alignment-based SNP calling or single-cell genome sequencing. For some species, the common SNP pool is expected to expand through additional genome sequencing. Third, a small number of species lacked species-specific sck-mers due to the presence of highly related species in the genome collection. Separate strategies such as using longer k-mers or less common SNPs could enable GT-Pro metagenotyping for these species. Fourth, although we were very selective in the choice of genomes and SNPs used for building GT-Pro, it is impossible to exclude all imperfections (e.g. incompleteness, contaminations and species misclassification) in the genome assemblies that could contribute to false SNP calls. Finally, GT-Pro does not directly genotype structural variants, which contribute significantly to intra-species genetic diversity[25]. However, we did show that GT-Pro can be used to impute insertions and deletions in high LD with common SNPs. Despite these caveats, we showed that the GT-Pro framework is general, accurate and sensitive for identifying genetic variation in metagenomes.

We envision several directions for future work. First, this study applied the GT-Pro approach to human gut prokaryotic species, and the framework could easily be expanded to other kingdoms and environments. Another extension is to develop alignment-free metagenotyping for short indels and structural variants. This study barely scratches the surface in terms of interpreting microbiome genetic variation. Towards leveraging microbiomes in precision medicine, it will be critical to comprehensively identify SNPs that are associated with disease and other traits (e.g. pathogenicity, antimicrobial resistance, drug degradation). We anticipate that GT-Pro will also be useful for detecting contamination, recombination, and horizontal gene transfer events, as well as tracking variants or strains over time, host lifestyle and geography.

Reference

1. Garud, N. R. & Pollard, K. S. Population Genetics in the Human Microbiome. *Trends Genet.* **36**, 53–67 (2020).
2. Maini Rekdal, V., Bess, E. N., Bisanz, J. E., Turnbaugh, P. J. & Balskus, E. P. Discovery and inhibition of an interspecies gut bacterial pathway for Levodopa metabolism. *Science* **364**, eaau6323 (2019).
3. Treangen, T. J., Ondov, B. D., Koren, S. & Phillippy, A. M. The Harvest suite for rapid core-genome alignment and visualization of thousands of intraspecific microbial genomes. *Genome Biol.* **15**, 524 (2014).
4. Schloissnig, S. *et al.* Genomic variation landscape of the human gut microbiome. *Nature* **493**, 45–50 (2013).
5. Luo, C. *et al.* ConStrains identifies microbial strains in metagenomic datasets. *Nat. Biotechnol.* **33**, 1045–1052 (2015).
6. Nayfach, S., Rodriguez-Mueller, B., Garud, N. & Pollard, K. S. An integrated metagenomics pipeline for strain profiling reveals novel patterns of bacterial transmission and biogeography. *Genome Res.* **26**, 1612–1625 (2016).
7. Costea, P. I. *et al.* metaSNV: A tool for metagenomic strain level analysis. *PLOS ONE* **12**, e0182392 (2017).
8. Quince, C. *et al.* DESMAN: a new tool for de novo extraction of strains from metagenomes. *Genome Biol.* **18**, 181 (2017).
9. Truong, D. T., Tett, A., Pasolli, E., Huttenhower, C. & Segata, N. Microbial strain-level population structure and genetic diversity from metagenomes. *Genome Res.* **27**, 626–638 (2017).
10. Wood, D. E. & Salzberg, S. L. Kraken: ultrafast metagenomic sequence classification using exact alignments. *Genome Biol.* **15**, R46 (2014).
11. Ounit, R., Wanamaker, S., Close, T. J. & Lonardi, S. CLARK: fast and accurate classification of metagenomic and genomic sequences using discriminative k-mers. *BMC Genomics* **16**, 236 (2015).
12. Liu, Y., Zhang, L. Y. & Li, J. Fast detection of maximal exact matches via fixed sampling of query K-mers and Bloom filtering of index K-mers. *Bioinformatics* **35**, 4560–4567 (2019).
13. Shajii, A., Yorukoglu, D., William Yu, Y. & Berger, B. Fast genotyping of known SNPs through approximate k-mer matching. *Bioinforma. Oxf. Engl.* **32**, i538–i544 (2016).
14. Parks, D. H., Imelfort, M., Skennerton, C. T., Hugenholtz, P. & Tyson, G. W. CheckM: assessing the quality of microbial genomes recovered from isolates, single cells, and metagenomes. *Genome Res.* **25**, 1043–1055 (2015).
15. Almeida, A. *et al.* A unified sequence catalogue of over 280,000 genomes obtained from the human gut microbiome. *bioRxiv* 762682 (2019) doi:10.1101/762682.
16. Pasolli, E. *et al.* Extensive Unexplored Human Microbiome Diversity Revealed by Over 150,000 Genomes from Metagenomes Spanning Age, Geography, and Lifestyle. *Cell* **176**, 649-662.e20 (2019).
17. Nayfach, S., Shi, Z. J., Seshadri, R., Pollard, K. S. & Kyrpides, N. C. New insights from uncultivated genomes of the global human gut microbiome. *Nature* **568**, 505–510 (2019).
18. Almeida, A. *et al.* A new genomic blueprint of the human gut microbiota. *Nature* **568**, 499–504 (2019).
19. Auton, A. *et al.* A global reference for human genetic variation. *Nature* **526**, 68–74 (2015).
20. Smits, S. A. *et al.* Seasonal cycling in the gut microbiome of the Hadza hunter-gatherers of Tanzania. *Science* **357**, 802 (2017).
21. Zou, Y. *et al.* 1,520 reference genomes from cultivated human gut bacteria enable functional microbiome analyses. *Nat. Biotechnol.* **37**, 179–185 (2019).
22. Turnbaugh, P. J. *et al.* The Human Microbiome Project. *Nature* **449**, 804–810 (2007).
23. Bäckhed, F. *et al.* Dynamics and Stabilization of the Human Gut Microbiome during the First Year of Life. *Cell Host Microbe* **17**, 852 (2015).

24. Franzosa, E. A. *et al.* Gut microbiome structure and metabolic activity in inflammatory bowel disease. *Nat. Microbiol.* **4**, 293–305 (2019).

25. Tierney, B. T. *et al.* The Landscape of Genetic Content in the Gut and Oral Human Microbiome. *Cell Host Microbe* **26**, 283-295.e8 (2019).

Figure legends

Figure 1. In sillico metagenotyping framework

Our method starts with a whole genome sequence collection and identifies species with sufficient high-quality genomes to call SNPs. For each species, a representative genome is chosen based on pairwise Average Nucleotide Identity (ANI) plus assembly quality metrics. SNPs are called per species based upon whole genome alignment of conspecific genomes to the representative genome. Common (MAF > 1%) bi-allelic SNPs are selected for genotyping. Up to 4 X k candidate k-mers are extracted per SNP site, covering both the reference and alternative allele on forward and reverse complementary strands (sck-mers; k=31 in this study). These candidate sck-mers are iteratively filtered through species-specificity filters of all unique k-mers present in the genomes of every other species, including species with insufficient high-quality genomes for genotyping. Only SNPs with sck-mers for both the reference and alternative allele are retained. SNPs are clustered based on pairwise linkage disequilibrium (LD). LD blocks are detected with a threshold of mean r2 > 0.81, and we select a tag SNP with species-specific sck-mers and the highest LD to other SNPs in the block. Optimized algorithms and compressed representations of sck-mer data enable rapid metagenotyping. Further details in Methods and Figure 3.

Figure 2. Genetic landscape of 909 human gut species.

(a) Summary of common SNP characteristics across all species (from left to right): at most SNPs only two alleles are observed, bi-allelic SNPs are mostly within protein-coding genes, these are largely synonymous, and the non-synonymous ones rarely disrupt or introduce a stop codon. (b and c) Phyla differ in their median SNP density and average LD block size with significant variation in density across species within each phylum. (d) Rate of LD distance decay across gut bacterial species. (b-e) are colored by bacterial phylum and share the same color scheme. (e) Examples of LD distance decay for individual species. From top to bottom are three species (species id: 102446, 101694 and 102831) with increasingly fast LD distance decay, suggesting higher recombination rates. Curves represent the fitted exponential decay model. (f) Visualization of two distinct haplotype landscapes from (upper) species *Alistipes putredinis* (species id: 101302) and (lower) *Bacteroides xylanisolvens* (species id: 101345). Base axis represents and is ordered by genomic coordinate. Color indicates magnitude of LD between pairs of SNPs. The examples have the same genomic span (10,000 bp). (g) Distribution across species of the percentage of SNPs that can be genotyped by GT-Pro either directly ("without LD blocks") or by imputation using genotyped tag SNPs ("with LD blocks"). For a typical species, ~75% of SNPs can be genotyped directly and ~95% can be imputed.

Figure 3. Computational performance evaluation of GT-Pro.

(a) Computational performance of GT-Pro in laptop (left) and server (right) environments across values for l (Bloom filter size parameter) and m (m-index size parameter). Color gradient: processing speed, circle size: peak RAM use, black box: optimal l and m for each computing environment. (b) Comparison of speed (upper) and peak RAM usage (lower) between GT-Pro and alignment-based metagenotyping (metaSNV and MIDAS; see methods). We ran GT-Pro on both server (green) and laptop (yellow) environments, while alignment-based methods were run only in the server (grey) environment due to not being optimized for personal computers. Peak RAM usage exceeds RAM needed to store the database due to intermediate calculations, such as applying filters.

Figure 4. Metagenotyping accuracy evaluation of GT-Pro using simulations.

Accuracy comparisons of GT-Pro and alignment-based metagenotyping across species based on reads simulated from isolate genomes with sequencing error. (a) False discovery rate at a combination of sequencing coverage ranged from 0.001x to 15x. Each observation is the result from a metagenome containing reads from one isolate. False discoveries are genotype calls that do not match the genome from which reads were simulated. (b) Sensitivity across coverage levels from the simulations in (a). Sensitivity is the probability of detecting SNPs present in the isolate genome. (c) False discovery rate at heterozygous sites in metagenomes containing reads from two isolates of each species. A combination of sequencing coverage ratio between two isolates was simulated by fixing a more abundant isolate at 15x coverage in all simulations, and varying the other isolate's coverage from 0.001x to 15x (coverage ratio = 0.001:15 to 15:15). (d) Sensitivity at heterozygous sites in metagenomes from (c). Sensitivity is the probability of correctly calling the heterozygous genotype of sites that differ between the genomes from which reads were simulated. (e) False discovery rate of genotypes imputed from tag SNPs based on allele matching in simulations in (a). Imputation is simply done by selecting the genotype associated with the observed tag SNP. (f) Sequencing coverage estimated using read counts at GT-Pro genotyped SNPs correlates with the simulated coverage, even when coverage is <1x. Each observation is the estimate from metagenomic reads simulated with sequencing error from a single isolate genome. (g) Sequencing coverage ratio estimates based on read counts for each allele at GT-Pro genotyped heterozygous sites correlate with the simulated ratios of two isolate genomes, even when one is much less abundant than the other (<=1:15). The more abundant isolate is at 15x coverage in all simulations.

Figure 5. Metagenotyping and gene imputation from gut metagenomes

Comparison of metagenotypes from GT-Pro and alignment with gut microbiome samples from a North America cohort[22] (HMP project; n=358; Table S8). As an example, we show the species *Bacteroides stercoris* (species id: 103681). Each point represents a SNP, with color indicating if the genotypes from the two methods agree (green), both methods return a genotype but the alleles disagree (purple), or only GT-Pro returns a genotype (black). Disagreements largely occur near 0.5 allele frequency, where small differences in read counts per allele can "flip" the major and minor alleles. (a) The proportion of samples in which each SNP is genotyped (prevalence) is similar with both methods. (b) Average allele frequency across samples varies across SNPs but is highly correlated between the two methods. (c and d) Comparison similar as (a and b) showing the species GCA_000431835.1 (genus: Succinivibrio, species id: 100412) from a different Madagascar cohort[16] (n=112; Table S9). Prediction of presence/absence of *C. difficile* pathogenic gene sets in human gut metagenomes from a mix of cohorts (n=7459) (Table S14) a random forest classifier built using GT-Pro SNPs from flanking regions in 117 *C. difficile* isolates (Figures S23-S24) with 10-fold cross validation. Heatmaps show the predicted (first column) and observed (based on alignment, second column) presence (black) or absence (white) in each sample (rows). Barplots show *C. difficile* relative abundance (left), whole genome sequence coverage (middle), and number of detected genes from the pathogeneticity locus (right), all estimated by mapping reads from each sample to a *C. difficile* representative genome. Random Forest predictions correlate with abundance, coverage, and number of detected pathogenic genes (Figure S25). (l) CdtLoc genes. (m) PaLoc genes.

Figure 6. Global genetic structure in 6,452 human gut metagenomes.

(a-d) Gut species differ in the amount of common SNP genetic diversity already present in sequenced genomes. Metagenomic samples from a North American IBD cohort[24] (n=220; Table S11) (purple) are visualized in two dimensions alongside the UHGG genomes (green). Each plot is the result of applying UMAP to a matrix of genotypes at GT-Pro SNPs for one species. Each dot represents a strain of that species (major allele for heterozygous metagenomes); those closer together in UMAP space have more similar genotypes. (a) *Anaerostipes hadrus* (species id: 102528) and (b) *Ruminococcus_B faecis* (species id: 100249) are species where metagenomes lie within the diversity previously captured by genomes. (c) *Blautia_A obeum* (species id: 100212) and (d) *Dialister invisus* (species id: 104158) are species where metagenomes harbor combinations of common SNPs outside the range present in genomes, which may represent novel subspecies. (e) Heatmap of mean allele sharing scores over all species between metagenomes from different pairs of countries. Crossed cells indicates missing scores due to insufficient (< 5000) pairs of samples. (f) Analysis of inter-continental population differentiation (FST) for 78 prevalent species. Each boxplot represents a distribution of inter-continental FST for one species, ordered by medians. (g) An example of geographic patterns captured by within-species genetic variation in the GT-Pro metagenotypes of specific species. Each dot is a metagenomic sample, colored by continents. Dimension reduction and visualization performed with UMAP. The example is from *Agathobacter rectalis* (species id: 102492). Nearby samples in UMAP space have similar abundance profiles; the absence of distinct groups indicates that relative abundance does not show strong geographic clustering. (h) UMAP analysis based on the relative abundances of the 881 GT-Pro species in the same samples as (i).

Figure 1

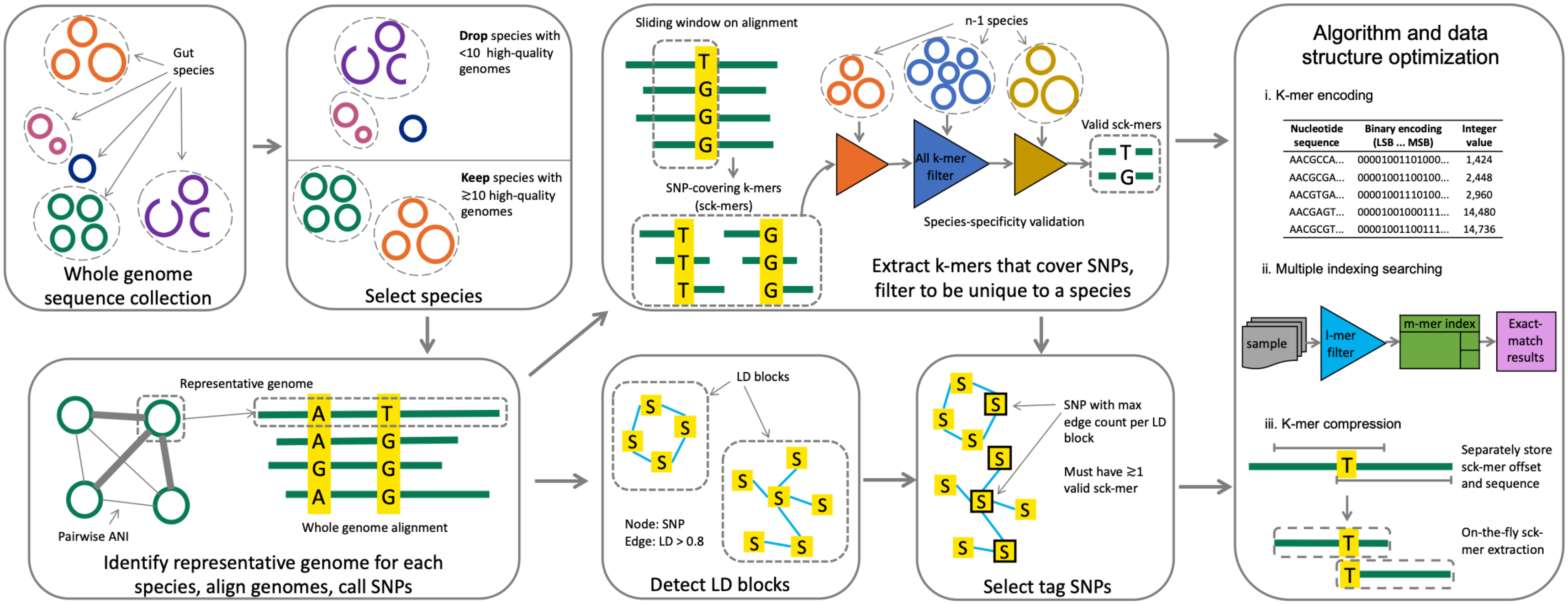
Gut species
Whole genome sequence collection
Drop species with <10 high-quality genomes
Keep species with ≥10 high-quality genomes
Select species
Representative genome
Pairwise ANI
Whole genome alignment
Identify representative genome for each species, align genomes, call SNPs
Sliding window on alignment
SNP-covering k-mers (sck-mers)
n-1 species
All k-mer filter
Valid sck-mers
Species-specificity validation
Extract k-mers that cover SNPs, filter to be unique to a species
LD blocks
Node: SNP
Edge: LD > 0.8
Detect LD blocks
SNP with max edge count per LD block
Must have ≥1 valid sck-mer
Select tag SNPs
Algorithm and data structure optimization
i. K-mer encoding
ii. Multiple indexing searching
sample
l-mer filter
m-mer index
Exact-match results
iii. K-mer compression
Separately store sck-mer offset and sequence
On-the-fly sck-mer extraction

Nucleotide sequence	Binary encoding (LSB ... MSB)	Integer value
AACGCCA...	00001001101000...	1,424
AACGCGA...	00001001100100...	2,448
AACGTGA...	00001001110100...	2,960
AACGAGT...	00001001000111...	14,480
AACGCGT...	00001001100111...	14,736

Figure 2

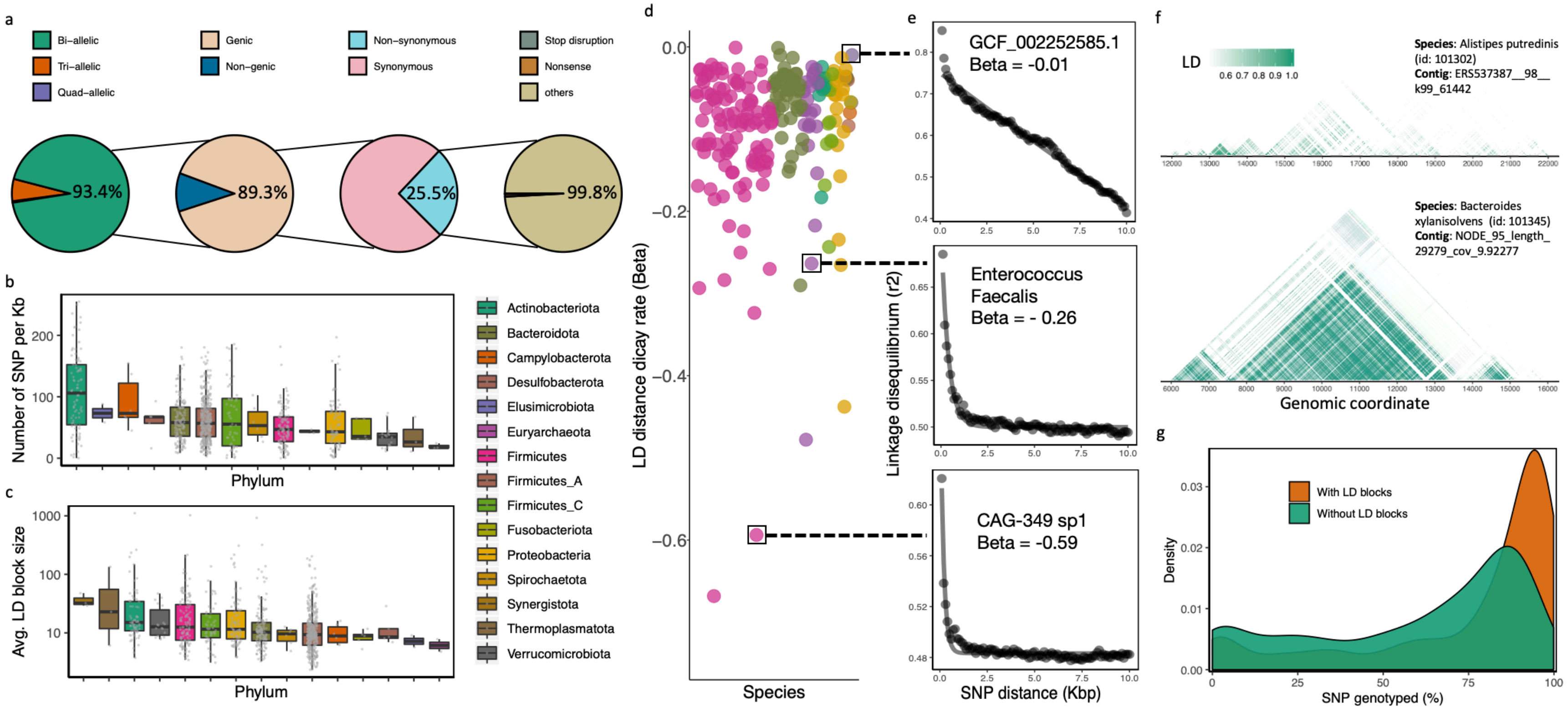
a
Bi–allelic
Tri–allelic
Quad–allelic
Genic
Non–genic
Non–synonymous
Synonymous
Stop disruption
Nonsense
others
93.4%
89.3%
25.5%
99.8%
b
Number of SNP per Kb
0
100
200
Phylum
c
Avg. LD block size
10
100
1000
Phylum
Actinobacteriota
Bacteroidota
Campylobacterota
Desulfobacterota
Elusimicrobiota
Euryarchaeota
Firmicutes
Firmicutes_A
Firmicutes_C
Fusobacteriota
Proteobacteria
Spirochaetota
Synergistota
Thermoplasmatota
Verrucomicrobiota
d
LD distance dicay rate (Beta)
0.0
−0.2
−0.4
−0.6
Species
e
GCF_002252585.1
Beta = -0.01
0.4
0.5
0.6
0.7
0.8
Enterococcus
Faecalis
Beta = - 0.26
0.50
0.55
0.60
0.65
CAG-349 sp1
Beta = -0.59
0.48
0.52
0.56
0.60
Linkage disequilibrium (r2)
0.0
2.5
5.0
7.5
10.0
SNP distance (Kbp)
f
LD
0.6 0.7 0.8 0.9 1.0
Species: Alistipes putredinis (id: 101302)
Contig: ERS537387__98__k99_61442
12000
13000
14000
15000
16000
17000
18000
19000
20000
21000
22000
Species: Bacteroides xylanisolvens (id: 101345)
Contig: NODE_95_length_29279_cov_9.92277
6000
7000
8000
9000
10000
11000
12000
13000
14000
15000
16000
Genomic coordinate
g
With LD blocks
Without LD blocks
Density
0.00
0.01
0.02
0.03
0
25
50
75
100
SNP genotyped (%)

Figure 3

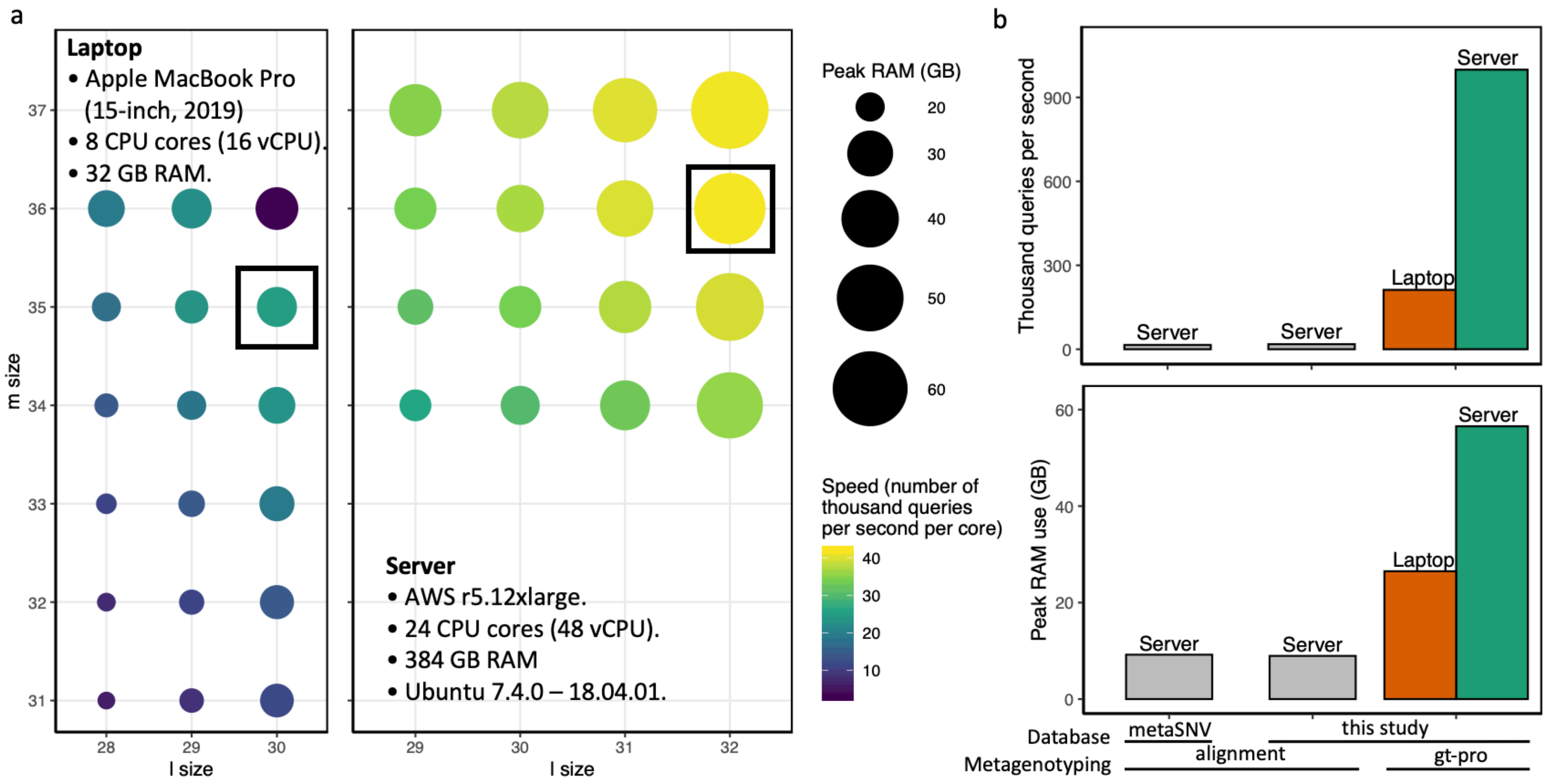
a
Laptop
• Apple MacBook Pro (15-inch, 2019)
• 8 CPU cores (16 vCPU).
• 32 GB RAM.
Server
• AWS r5.12xlarge.
• 24 CPU cores (48 vCPU).
• 384 GB RAM
• Ubuntu 7.4.0 – 18.04.01.
m size
31
32
33
34
35
36
37
l size
28
29
30
31
32
Peak RAM (GB)
20
30
40
50
60
Speed (number of thousand queries per second per core)
10
20
30
40
b
Thousand queries per second
0
300
600
900
Peak RAM use (GB)
0
20
40
60
Server
Server
Laptop
Server
Database
metaSNV
this study
Metagenotyping
alignment
gt-pro

Figure 4

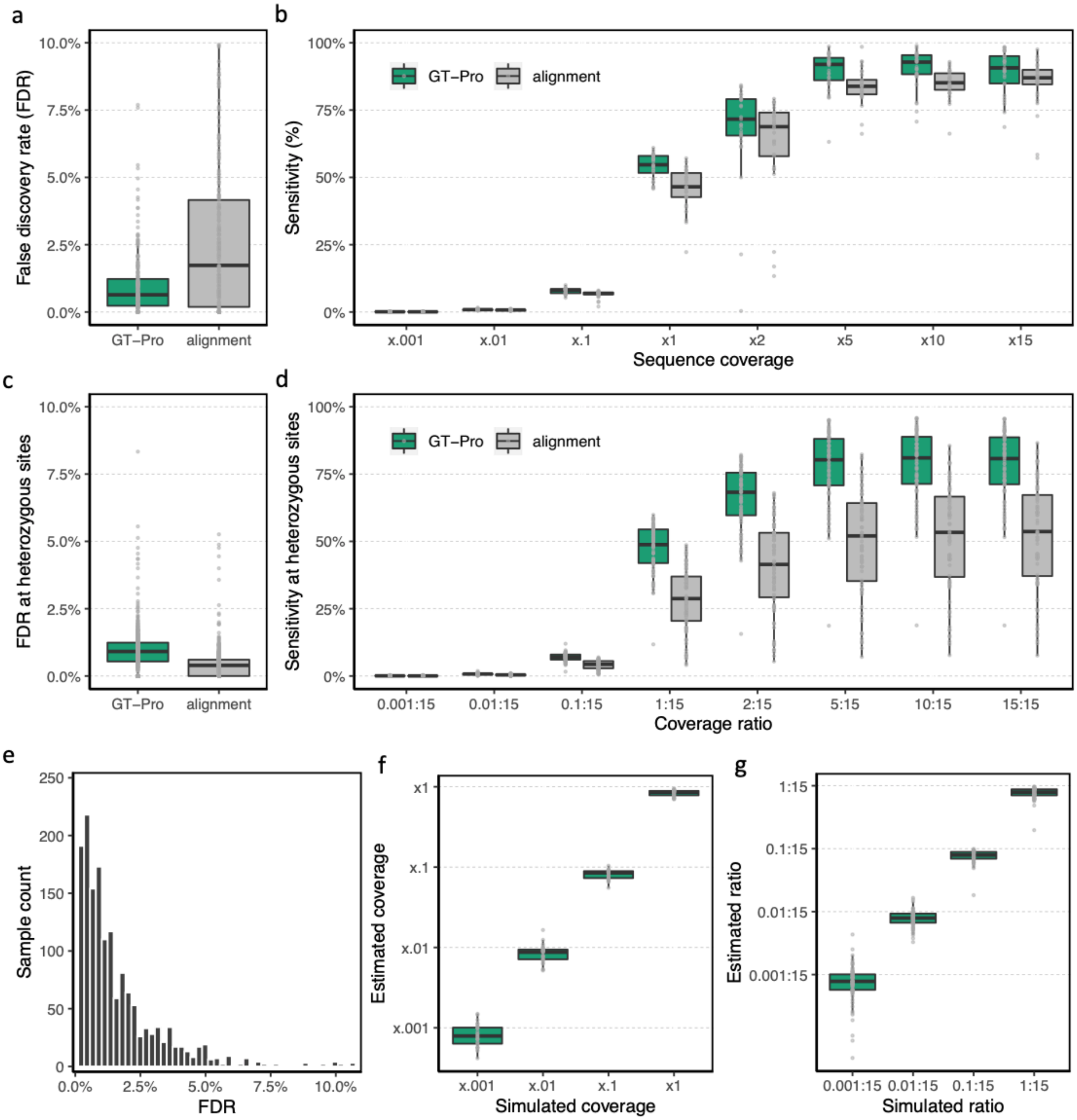
a
False discovery rate (FDR)
10.0%
7.5%
5.0%
2.5%
0.0%
GT−Pro
alignment
b
Sensitivity (%)
100%
75%
50%
25%
0%
GT−Pro
alignment
x.001
x.01
x.1
x1
x2
x5
x10
x15
Sequence coverage
c
FDR at heterozygous sites
10.0%
7.5%
5.0%
2.5%
0.0%
GT−Pro
alignment
d
Sensitivity at heterozygous sites
100%
75%
50%
25%
0%
GT−Pro
alignment
0.001:15
0.01:15
0.1:15
1:15
2:15
5:15
10:15
15:15
Coverage ratio
e
Sample count
250
200
150
100
50
0
0.0%
2.5%
5.0%
7.5%
10.0%
FDR
f
Estimated coverage
x1
x.1
x.01
x.001
x.001
x.01
x.1
x1
Simulated coverage
g
Estimated ratio
1:15
0.1:15
0.01:15
0.001:15
0.001:15
0.01:15
0.1:15
1:15
Simulated ratio

Figure 5

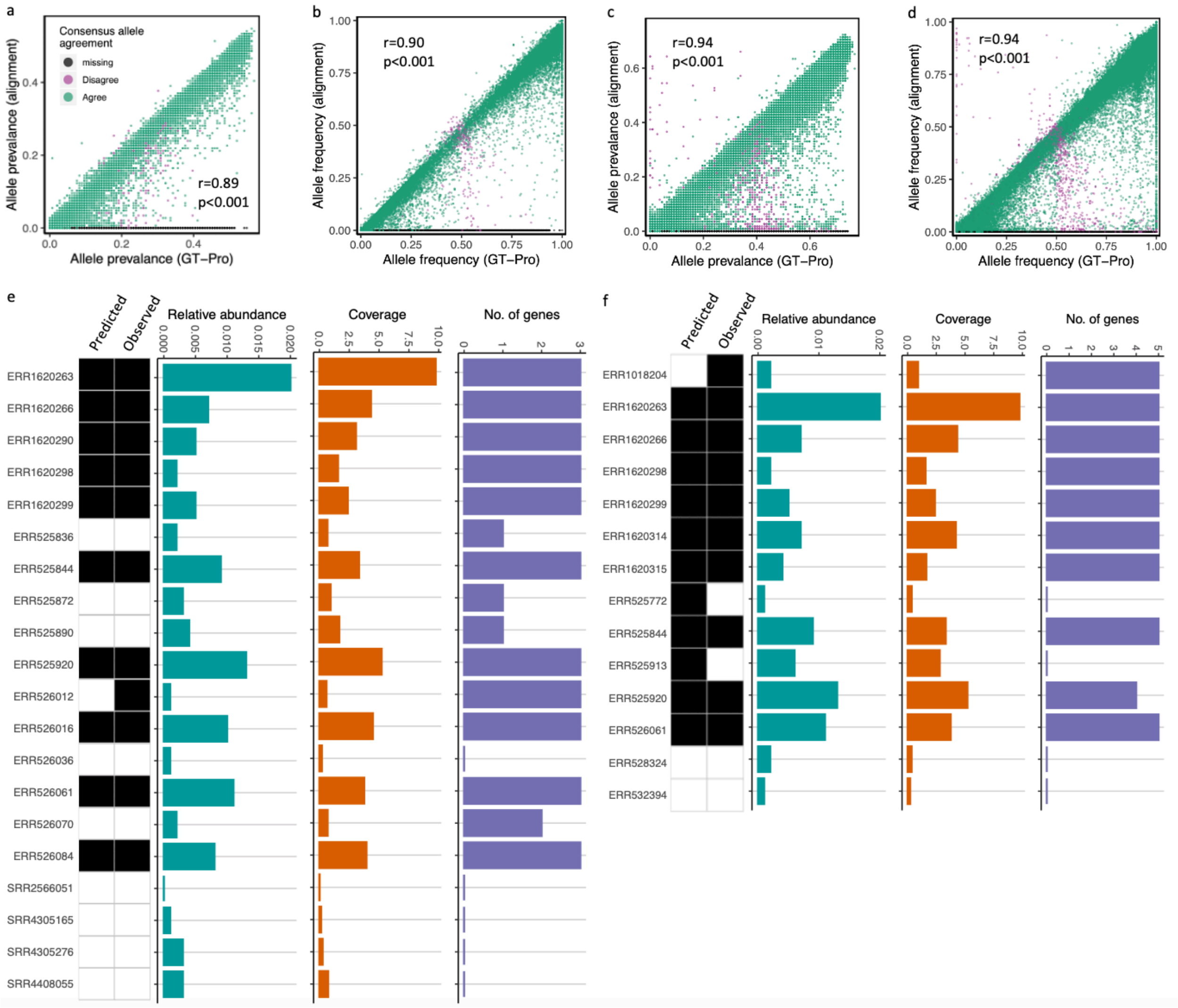
a
Consensus allele agreement
missing
Disagree
Agree
r=0.89
p<0.001
Allele prevalance (alignment)
Allele prevalance (GT−Pro)
0.0
0.2
0.4
b
r=0.90
p<0.001
Allele frequency (alignment)
Allele frequency (GT−Pro)
0.00
0.25
0.50
0.75
1.00
c
r=0.94
p<0.001
Allele prevalance (alignment)
Allele prevalance (GT−Pro)
0.0
0.2
0.4
0.6
d
r=0.94
p<0.001
Allele frequency (alignment)
Allele frequency (GT−Pro)
0.00
0.25
0.50
0.75
1.00
e
Predicted
Observed
Relative abundance
0.000
0.005
0.010
0.015
0.020
Coverage
0.0
2.5
5.0
7.5
10.0
No. of genes
0
1
2
3
ERR1620263
ERR1620266
ERR1620290
ERR1620298
ERR1620299
ERR525836
ERR525844
ERR525872
ERR525890
ERR525920
ERR526012
ERR526016
ERR526036
ERR526061
ERR526070
ERR526084
SRR2566051
SRR4305165
SRR4305276
SRR4408055
f
Predicted
Observed
Relative abundance
0.00
0.01
0.02
Coverage
0.0
2.5
5.0
7.5
10.0
No. of genes
0
1
2
3
4
5
ERR1018204
ERR1620263
ERR1620266
ERR1620298
ERR1620299
ERR1620314
ERR1620315
ERR525772
ERR525844
ERR525913
ERR525920
ERR526061
ERR528324
ERR532394

Figure 6

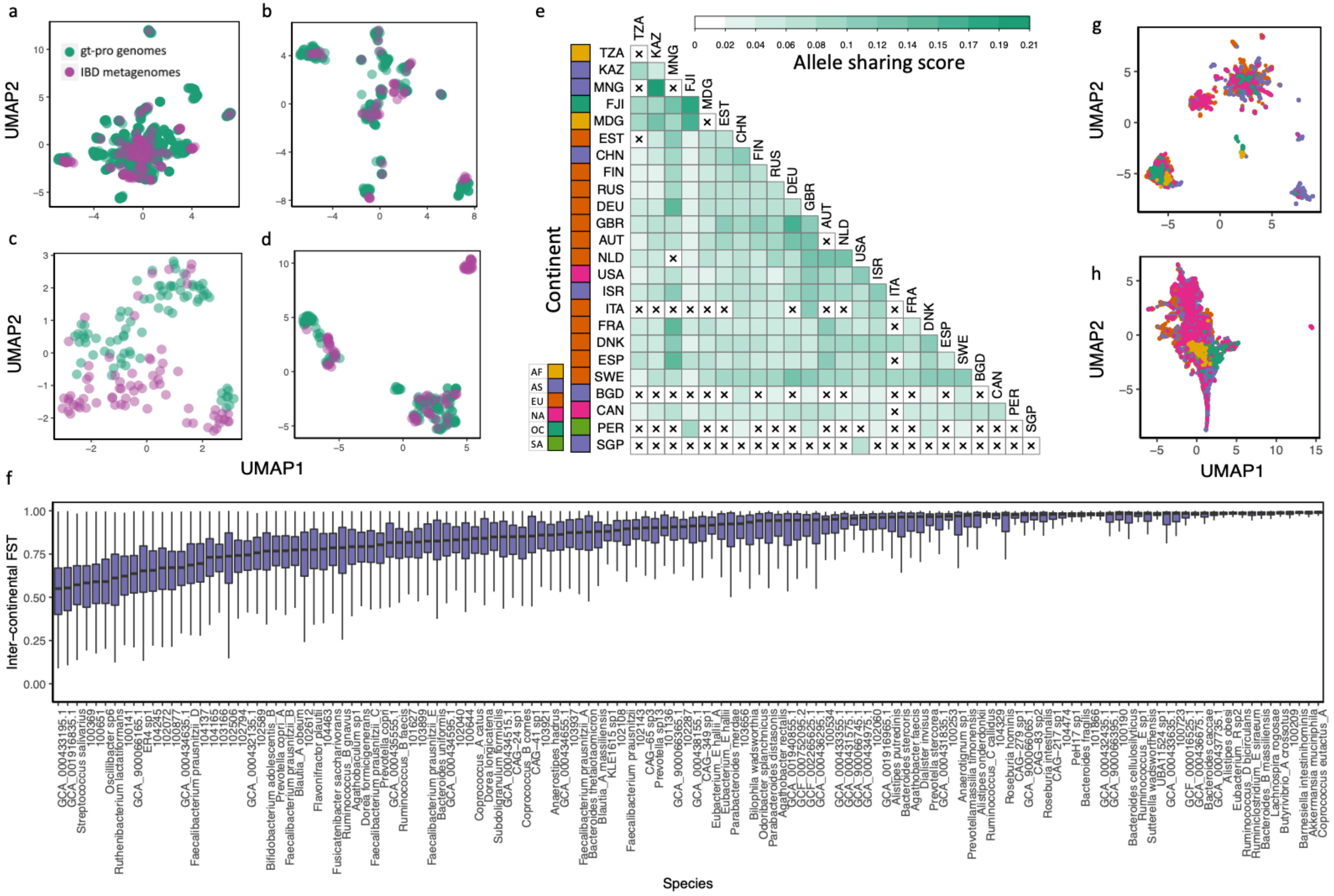
a
gt-pro genomes
IBD metagenomes
UMAP2
10
5
0
−5
−4
0
4
b
4
0
−4
−8
−4
0
4
8
c
UMAP2
3
2
1
0
−1
−2
−2
0
2
d
10
5
0
−5
−5
0
5
UMAP1
e
Allele sharing score
0
0.02
0.04
0.06
0.08
0.1
0.12
0.14
0.15
0.17
0.19
0.21
Continent
TZA
KAZ
MNG
FJI
MDG
EST
CHN
FIN
RUS
DEU
GBR
AUT
NLD
USA
ISR
ITA
FRA
DNK
ESP
SWE
BGD
CAN
PER
SGP
AF
AS
EU
NA
OC
SA
g
UMAP2
5
0
−5
−5
0
5
h
UMAP2
5
0
−5
−5
0
5
10
15
UMAP1
f
Inter−continental FST
1.00
0.75
0.50
0.25
0.00
Species
GCA_000433195.1
GCA_001916835.1
Streptococcus salivarius
100369
100651
Oscillibacter sp6
Ruthenibacterium lactatiformans
100141
GCA_900066165.1
ER4 sp1
104245
102072
100877
GCA_000434635.1
Faecalibacterium prausnitzii_D
104137
104165
103166
102506
102794
GCA_000432135.1
102589
Bifidobacterium adolescentis_B
Prevotella copri_A
Faecalibacterium prausnitzii_B
Blautia_A obeum
102612
Flavonifractor plautii
104463
Fusicatenibacter saccharivorans
Ruminococcus_B gnavus
Agathobaculum sp1
Dorea formicigenerans
Faecalibacterium prausnitzii_C
Prevotella copri
GCA_000435555.1
Ruminococcus_B faecis
101627
103899
Faecalibacterium prausnitzii_E
Bacteroides uniformis
GCA_000434595.1
102040
100644
Coprococcus_A catus
Dorea longicatena
Subdoligranulum formicilis
GCA_000434515.1
CAG−24 sp1
Coprococcus_B comes
CAG−41 sp1
103921
Anaerostipes hadrus
GCA_000434655.1
103937
Faecalibacterium prausnitzii_A
Bacteroides thetaiotaomicron
Blautia_A massiliensis
KLE1615 sp1
102108
Faecalibacterium prausnitzii
102143
CAG−65 sp3
Prevotella sp13
101136
GCA_900066365.1
102287
GCA_000438155.1
CAG−349 sp1
Eubacterium_E hallii_A
Eubacterium_E hallii
Parabacteroides merdae
103656
Bilophila wadsworthia
Odoribacter splanchnicus
Parabacteroides distasonis
Agathobacter rectalis
GCA_001940855.1
GCF_000752095.2
GCF_002265625.1
GCA_000436295.1
100534
GCA_000433355.1
GCA_000431575.1
GCA_900066745.1
GCA_000434975.1
102060
GCA_001916965.1
Alistipes putredinis
Bacteroides stercoris
Agathobacter faecis
Dialister invisus
Prevotella stercorea
GCA_000431835.1
100253
Anaerotignum sp1
Prevotellamassilia timonensis
Alistipes onderdonkii
Ruminococcus_C callidus
104329
Roseburia hominis
CAG−279 sp1
GCA_900066065.1
CAG−83 sp2
Roseburia intestinalis
CAG−217 sp1
104474
PeH17 sp1
Bacteroides fragilis
101866
GCA_000432435.1
GCA_900066395.1
100190
Bacteroides cellulosilyticus
Ruminococcus_E sp1
Sutterella wadsworthensis
UBA11524 sp1
GCA_000433635.1
100723
GCF_000016525.1
GCA_000436675.1
Bacteroides caccae
GCA_000437735.1
Alistipes obesi
Eubacterium_R sp2
Ruminococcus_D bicirculans
Ruminiclostridium_E siraeum
Bacteroides_B massiliensis
Lachnospira rogosae
Butyrivibrio_A crossotus
100209
Barnesiella intestinihominis
Akkermansia muciniphila
Coprococcus eutactus_A